nature neuroscience

Propagating waves mediate information transfer in the motor cortex

Doug Rubino[1], Kay A Robbins[2] & Nicholas G Hatsopoulos[1]

High-frequency oscillations in the beta range (10–45 Hz) are most active in motor cortex during motor preparation and are postulated to reflect the steady postural state or global attentive state of the animal. By simultaneously recording multiple local field potential signals across the primary motor and dorsal premotor cortices of monkeys (*Macaca mulatta*) trained to perform an instructed-delay reaching task, we found that these oscillations propagated as waves across the surface of the motor cortex along dominant spatial axes characteristic of the local circuitry of the motor cortex. Moreover, we found that information about the visual target to be reached was encoded in terms of both latency and amplitude of evoked waves at a time when the field phase-locked with respect to the target onset. These findings suggest that high-frequency oscillations may subserve intra- and inter-cortical information transfer during movement preparation and execution.

Beta oscillations in electroencephalogram (EEG) and local field potentials (LFPs), observed across the sensorimotor cortex of both human and non-human primates, increase in power during movement planning or steady postural configurations and attenuate at movement initiation that is either cued or self-paced[1–6]. These oscillations also occur sporadically throughout behavioral tasks that require increased attention and active participation[7–10]. These findings suggest that beta activity may signal global aspects of motor planning and behavior such as attention or arousal.

Beta oscillations are believed to represent the summed activity of multiple, synchronous postsynaptic potentials near the electrode site. However, very little is known about their spatiotemporal properties across the surface of the motor cortex. Although synchronous or nearly synchronous activity with small, non-systematic temporal phase shifts between oscillations are observed at different cortical sites horizontally[7,9], no evidence for spatiotemporal structure within motor cortex has been found except for a decrease in correlation strength with inter-electrode distance[9]. Here we report that beta oscillations propagated as waves across the primary motor (MI) and premotor (PMd) cortices as monkeys planned and executed an instructed-delay reaching task. These waves propagated predominantly in one of two oppositely oriented directions in each cortical area. The dominant directions were consistent with the underlying structure of the local transcortical circuitry of the motor cortex, suggesting intra-cortical and inter-cortical communication between nearby cytoarchitectonic areas. Moreover, after the onset of the visual stimulus instructing the upcoming reaching movement, the beta oscillations were found to transiently phase-lock to the instruction stimulus, which generated evoked waves propagating along the dominant propagating axis of the on-going LFP waves. The latency and amplitude of these evoked waves varied systematically with target direction, indicating that propagating waves carry behaviorally relevant information.

RESULTS

Power in the beta band during movement planning

Monkeys were trained to perform an instructed-delay reaching task to one of eight targets. During the instruction period, a visual stimulus appeared instructing the animal where its upcoming movement should occur. The animal was trained not to move until the presentation of a 'go cue' signaling the initiation of the instructed movement. As others have shown[1,2,7], power spectra of the simultaneously recorded LFPs across multiple electrodes on the array revealed a dominant beta frequency band during the instruction period (**Fig. 1a**). By applying a band-pass filter (10–45 Hz) to the raw LFP signal (**Fig. 1b**, top), we isolated the beta oscillations (**Fig. 1b**, middle) and separated them from the slower fluctuations (**Fig. 1b**, bottom). Mean frequencies across monkeys ranged from 20 to 25 Hz.

As previously shown[7], beta power increased during movement planning and was most prominent 50–200 ms after the onset of the instruction stimulus. Beta power remained elevated from surrounding frequencies throughout the remainder of the instruction period and then dramatically attenuated around the onset of movement (**Fig. 1c**,**d**).

Beta waves in the motor cortex

Across a set of spatially separated electrodes in MI, the oscillatory peaks within one cycle of the beta oscillation occurred at different times, suggesting wave propagation (**Fig. 2a**). A phase map of the LFP across the entire two-dimensional array was computed using the Hilbert transform (Methods) and temporally averaged over one beta cycle

[1]Department of Organismal Biology and Anatomy, University of Chicago, Chicago, Illinois 60637, USA. [2]Department of Computer Science, University of Texas San Antonio, San Antonio, Texas 78249, USA. Correspondence should be addressed to N.G.H. (nicho@uchicago.edu).

Received 6 September; accepted 25 October; published online 19 November 2006; doi:10.1038/nn1802

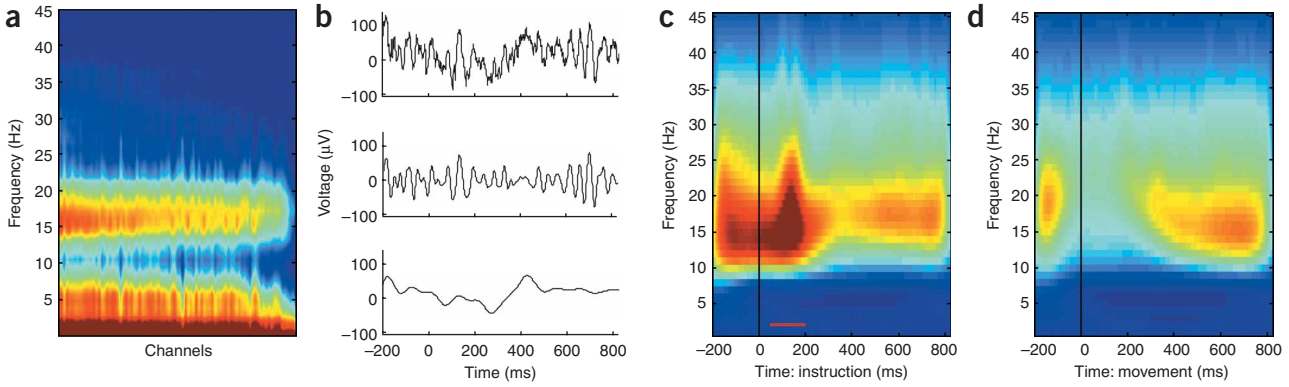

Figure 1 Time-frequency analysis of local field potentials in the motor cortex during the instructed-delay reaching task. (**a**) Power spectra during the instruction epoch, computed across all channels of the microelectrode array. Log power is presented in blue-red false color, and channels are sorted according to power in the beta range (10 to 45 Hz). (**b**) Top, an unfiltered LFP from a single electrode taken from data collected during the instructed-delay epoch of a single trial of the task. Middle, same as above, band-pass filtered at 10-45 Hz. Bottom, the same LFP low-pass filtered at 10 Hz. (**c**) Averaged wavelet spectrogram computed with respect to onset of the instruction stimulus. Power is presented in blue-red false color. Spectrograms were computed independently for each channel of each trial and averaged. (**d**) Same as **c** except computed with respect to the movement onset. The vertical lines in **c** and **d** mark the onset of the instruction stimulus and movement onset, respectively. All data presented are from monkey Rs from an array implanted in the primary motor cortex (MI).

(vertical red lines in **Fig. 2a**). The averaged phase revealed that the phase of the beta oscillations varied systematically across the array, which is evidence of a propagating wave (**Fig. 2b**). As seen from a series of time snapshots, this particular wave began in the upper left quadrant of the array and propagated at a mean velocity of 28 cm s^{-1} diagonally to the bottom right (**Fig. 2c**).

To quantitatively verify that coordinated spatial activity occurred continuously throughout the instruction epoch, we computed the spatial coherence of the LFPs across arrays implanted in MI (**Fig. 3a**, top and middle) and PMd (**Fig. 3a**, bottom) over all trials, which revealed a peak between 10 and 45 Hz corresponding to the beta range of oscillations typically observed in motor cortex during preparation to move. To specifically verify that the data were behaving like propagating waves, we computed the phase-gradient directionality (PGD) over the same data (Methods). PGD assesses the degree of alignment of the phase gradients across the array. The peak of the PGD spectrum was always present in the beta frequency range across all monkeys, suggesting that beta was the most wavelike frequency band below 100 Hz (**Fig. 3b**).

For each instance of time during the instruction epoch (every 1 ms), we generated an instantaneous phase map, from which the instantaneous propagation velocity was computed by spatially averaging the phase gradient. Data with high PDG values have a well defined propagation velocity, and therefore only data with instantaneous PGD values greater than 0.5 were included in this velocity analysis. The distributions of the speeds of propagating waves during the instruction epoch were single peaked (**Fig. 3c**). Mean propagation speeds ranged between 12 and 26 cm s^{-1} over all monkeys. Given a propagation speed of 20 cm s^{-1} and a temporal frequency of 20 Hz, the wavelength of the propagating beta activity was 10 mm, which is comparable to the linear dimension of the arm area of MI.

We also computed the distributions of propagation directions from the same data (**Fig. 4a**). Peaks in the propagation direction distributions revealed the most frequent propagation directions of the beta waves, which we term the dominant propagation directions. We observed two

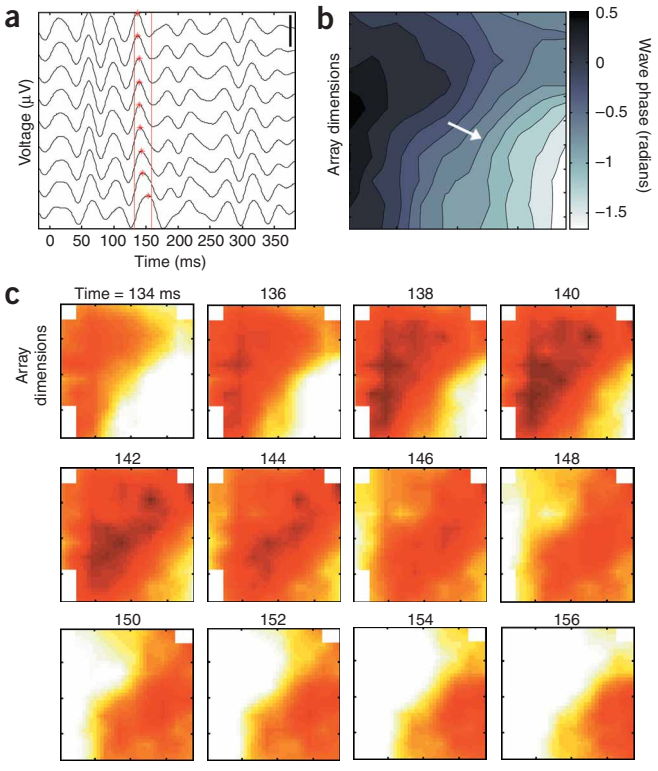

Figure 2 Wave propagation in the beta frequency range. Data are from a single trial in MI of monkey Rx. (**a**) Local field potentials in the beta band along the diagonal electrodes of the array. Red stars mark the local maxima of one characteristic beta cycle, and the red lines mark the beginning and end of the wave snapshots presented in **c**. Scale bar, 500 μV. (**b**) Average phase of the beta wave marked in **a** plotted with respect to the multi-electrode array dimensions. Phase is presented using contour lines in black-white false color. Six missing data points were interpolated for continuity before averaging. The white arrow indicates direction of wave propagation. (**c**) Individual time snapshots of the voltages corresponding to the wave shown in **a** and **b**, plotted with respect to the dimensions of the multi-electrode array. Time (in milliseconds) is labeled above each plot, with time zero corresponding to the onset of the instruction stimulus. Voltage is presented in white-red false color (red indicating positive voltage). This particular wave took approximately 20 ms to propagate across the 4 × 4 mm array.

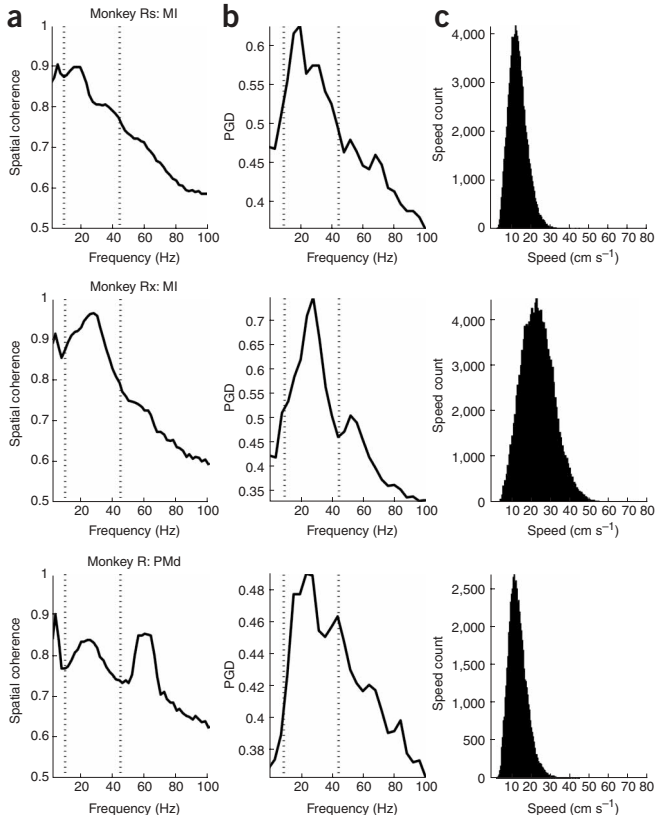

Figure 3 Spatial coherence, phase gradient directionality (*PGD*) and wave speed. Data from monkey Rs, MI (top), monkey Rx, MI (middle) and monkey R, PMd (bottom). (**a**) Spatial coherence as a function of frequency for unfiltered LFP signals across the array, averaged over all trials during the instruction epoch. The dotted vertical lines mark the 10 and 45 Hz boundaries of the beta band used to band-pass filter the LFP signals for further analysis. The second peak in coherence in the bottom panel is due to 60 cycle line noise. (**b**) *PGD* as a function of frequency for band-pass filtered LFPs (bandwidth 10 Hz) from 0 to 100 Hz. *PGD* values were averaged over all trials and times per frequency. The dotted vertical lines mark the 10 and 45 Hz boundaries of the beta band used to band-pass filter the LFP signals for further analysis. (**c**) Histograms of the wave propagation speeds during the instruction period for 10–45 Hz beta activity with PGD > 0.5.

dominant propagation directions (a primary and secondary propagation direction), which were approximately 180° apart, comprising a dominant propagation axis. Average phase maps using data associated with the primary (**Fig. 4b**) and secondary (**Fig. 4c**) peaks revealed the spatial dynamics of the two dominant propagating wave directions. The dominant propagation directions were consistent across monkeys, showing an anterior-posterior dominant propagation axis in MI and a medial-lateral dominant propagation axis in PMd (**Fig. 5**). Even though oscillatory power in the beta range strongly attenuated after the initiation of movement, beta activity continued to propagate as waves and displayed the same dominant propagation directions as during the instruction epoch (**Supplementary Fig. 1** online).

We computed wave propagation velocities separately using two methods: the first method applied the Hilbert transform to compute instantaneous phase, and the second method applied Slepian tapers and singular-value decomposition to Fourier-transformed data. The results were similar (**Supplementary Fig. 2** online), but the Hilbert transform-based method seemed to be less sensitive to noise, and, therefore, we analyzed only results based on the Hilbert transform-based method for information content.

Phase-locked beta waves

During the 50 to 200 ms time interval after the onset of the instruction stimulus, during which power in the beta band increased (**Fig. 1c**, red line), we observed a time-locked evoked potential[11] (**Fig. 6a**, top and middle). To assess the degree of stimulus-related phase-locking, we computed the percent phase-locking (PPL) across trials (Methods). The LFP signal exhibited a strong degree of phase-locking during this

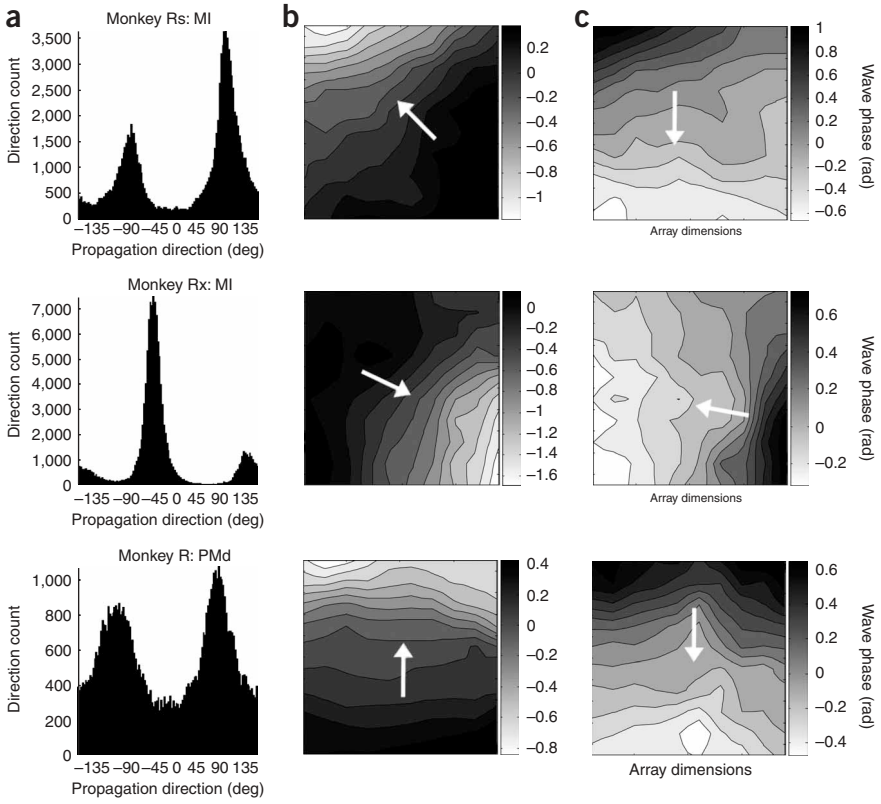

Figure 4 The direction of propagating waves during the instruction epoch. Data from monkey Rs, MI (top), monkey Rx, MI (middle) and monkey R, PMd (bottom). (**a**) Histogram of wave propagation directions during the instruction epoch of all trials for all times at which *PGD* > 0.5. (**b**) The average phase map, computed using the instantaneous phases from data with propagation directions within 45° of the highest peak in the histograms from **a**. The data are presented with respect to the array dimensions, and phase is presented in black-white false color. The arrow indicates the propagation direction of the waves, based on the direction of the negative phase gradient of the average phase map. (**c**) Same as in **b**, but using data with propagation directions within 45° of the second peak in the propagation direction histograms.

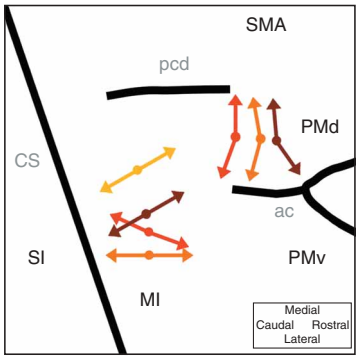

Figure 5 Dominant propagation directions of the beta waves on the cortical surface with respect to sulcal landmarks. The two clusters of arrows represent dominant propagation directions in the primary motor cortex and the dorsal premotor cortex, respectively. Data from monkey B are presented in orange, monkey R in red, monkey Rs in dark red, and monkey Rx in yellow. ac, arcuate sulcus. CS, central sulcus. pcd, precentral dimple. MI, primary motor cortex. PMd, dorsal premotor cortex. PMv, ventral premotor cortex. SI, primary somatosensory cortex. SMA, supplementary motor area.

period (**Fig. 6a**, bottom). The observed temporal phase-locking with the instruction cue was significantly larger during the 50 to 200 ms interval after instruction onset as compared to a 200 ms interval before the instruction onset on all electrodes in both MI and PMd in three of the four monkeys ($P < 0.01$, *t*-test; **Fig. 6b**). In the remaining monkey (monkey Rx), we found weak but insignificant phase-locking during that same 150 ms time interval.

PGD averaged across trials revealed that LFP activity behaved more like a single propagating wave during phase-locking (**Fig. 6c**), and average phase maps computed over evoked LFP data during that time interval showed that phase varied systematically across the array during the same time interval (**Fig. 6d**). The wave activity was consistent with the dominant wave axis. Because phase-locking of the LFP on one electrode implies the existence of an evoked potential, phase locking across electrodes with systematic shifts in phase angle implies the existence of evoked waves.

Information content in the evoked waves

By examining the evoked waves as a function of the instructed movement direction, we found systematic differences that suggested that task-related information was contained in the evoked waves. To assess this quantitatively, we computed mutual information between various features of the LFP waves and the target direction at multiple time points.

During the evoked potential (**Fig. 7a**,**b**), we found two independent sources of target information. First, target information was evident in the form of a latency code in both cortical areas. This was assessed by computing the mutual information between the instantaneous phase of the LFP (thereby ignoring amplitude) and the target direction over the instruction epoch (**Fig. 7c**). Phase provided significant transient target information during the evoked wave. That is, we observed systematic shifts in the latency of the evoked waves when targets associated with

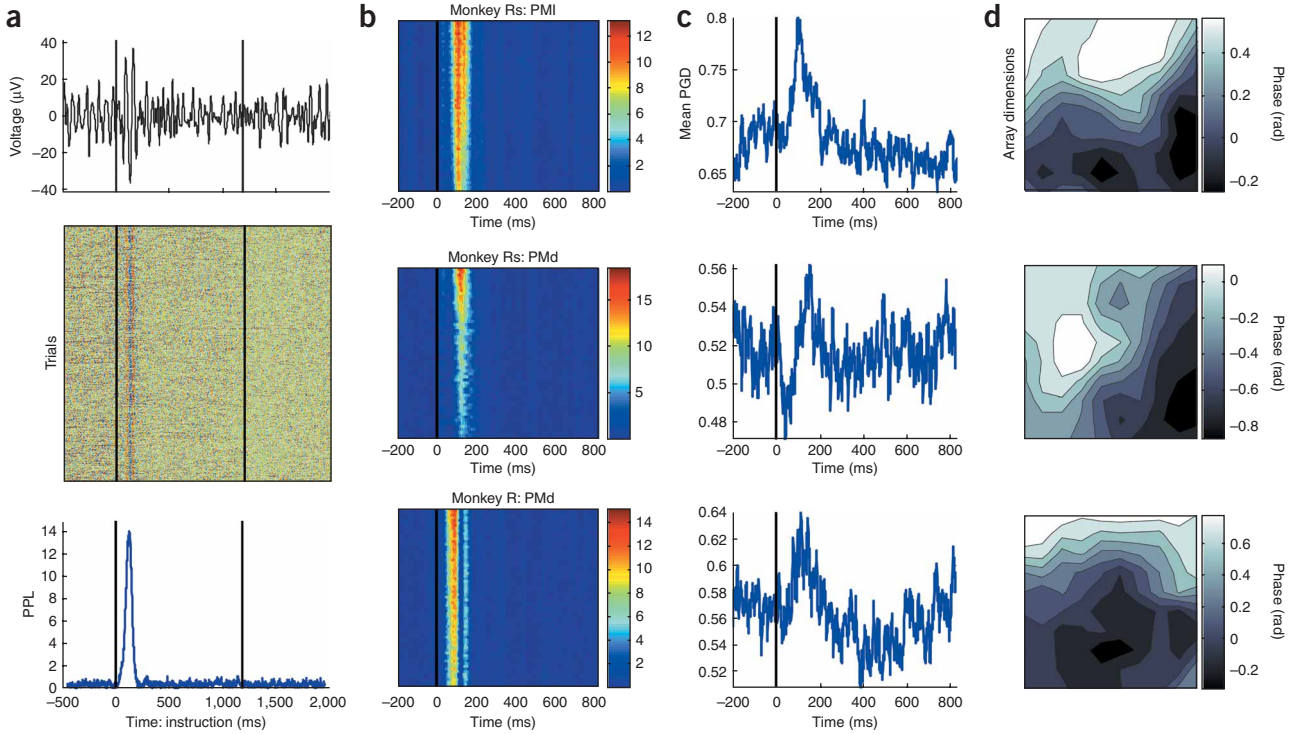

Figure 6 Waves evoked by the instruction stimulus. (**a**) Top, a stereotypical beta band LFP taken from one channel in one trial of a PMd array in monkey Rs. Time is presented on the horizontal axis. The first vertical line marks the time of the instruction cue, the second marks the onset of the go cue. Middle, same electrode used in **a**, with data taken from all trials of a single recording session. Voltage is presented in blue-red false color. Bottom, percent phase-locking (*PPL*) computed across time for the data above (Methods). (**b**) *PPL* computed across all channels during the instruction. Time is presented on the horizontal axis, and channels are presented on the vertical axis, sorted by maximum *PPL*. *PPL* is displayed using blue-red false color. (**c**) Phase gradient directionality (PGD) averaged across trials as a function of time with respect to the instruction cue. (**d**) Average phase maps for the evoked potentials, during the time of maximum *PPL* (50 to 200 ms after instruction stimulus onset). Phase is represented in a black-white scale and presented with respect to the spatial dimensions of the array. (**b–d**) Data collected from different monkeys and cortical areas: monkey Rs, MI (top); monkey Rs, PMd (middle); monkey R, PMd (bottom).

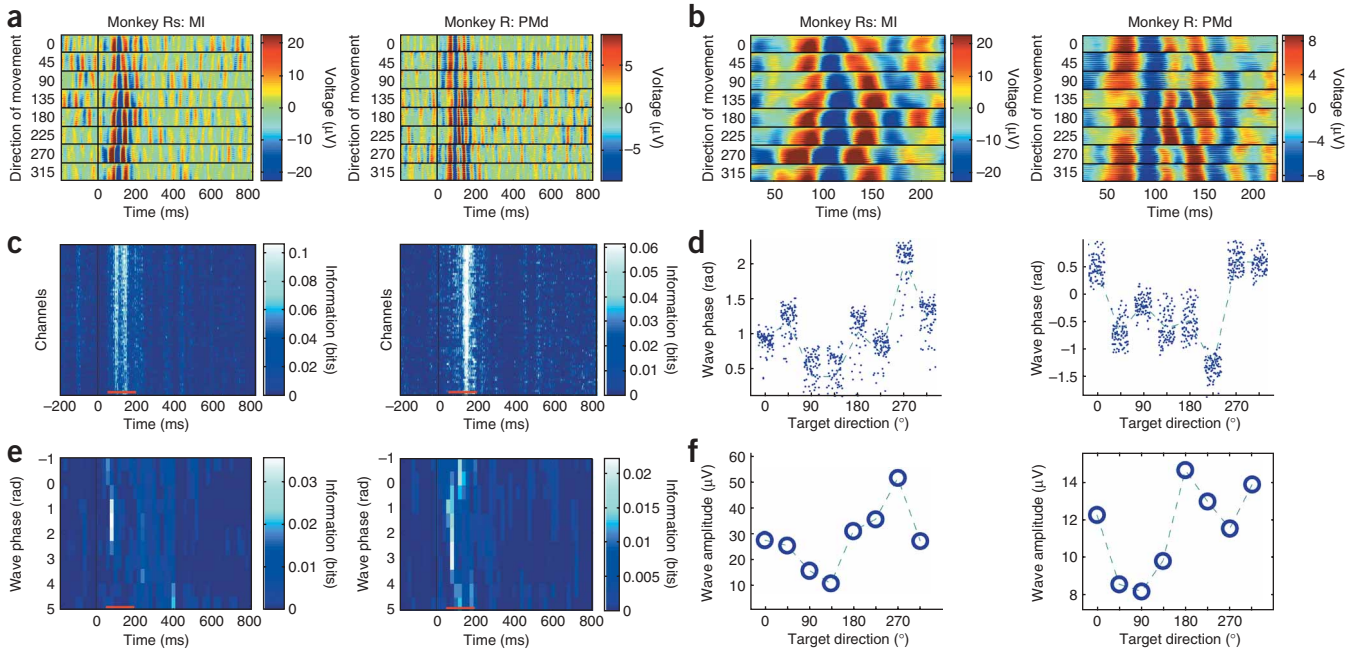

Figure 7 Information content of instruction stimulus-evoked waves in the beta band. Left in all panels, data from MI in monkey Rs. Right in all panels, data from PMd in monkey R. (**a**) Mean local field potentials in the beta band of the instruction epoch as a function of target direction. The graph consists of eight subpanels corresponding to the eight target directions (degrees), each with time on the horizontal axis, array channels on the vertical axis, and voltage in blue-red false color. (**b**) Same data presented in **a**, with time restricted to the first 200 ms following the presentation of the instruction cue, during which the evoked waves occur. (**c**) Wave-phase information, computed across channels and time. Wave-phase information is presented in blue-white false color in bits. The horizontal red line marks the duration of the evoked potential. (**d**) Single-channel LFP phases at the time of maximal wave-phase information of **c**. Each point represents a phase from a single channel on the array. (**e**) Wave-amplitude information, plotted as a function of wave-phase and time. Amplitude information is presented in blue-white false color in bits. Each pixel represents the information carried in the amplitudes at a particular phase of the waves in a 40 ms time bin. (**f**) Mean wave amplitudes at the time and phase of maximal wave-amplitude information in **e**. For **c** and **e**, the center value of the color axis was set to be the computed significant information threshold ($P = 0.01$; Methods).

different movement directions were presented 50–200 ms after the onset of the instruction stimulus (**Fig. 7d**).

Second, target information was also contained in the amplitude of the LFP oscillation, forming an independent amplitude code. Because amplitude varies continuously with phase in an oscillating signal, the amplitude had to be compared at the same phase across different target conditions. Therefore, amplitude was computed in time at particular phases of the LFP oscillation (**Fig. 7e**). As with phase (that is, latency) information, significant amplitude information occurred transiently during the evoked wave. This was evident in the differences in amplitude across different target conditions, for the phase that contained the most information (**Fig. 7f**). Although both latency and amplitude provided significant target information, the average information provided by latency was, in general, three times larger than that provided by amplitude during the instruction. No significant information was present either after the go cue or around the start of movement (n.s., shuffle test; Methods). We also found no significant mutual information between target direction and wave direction or wave speed during the instruction period, after the go cue, or around movement onset (n.s., shuffle test).

Our standard instructed-delay reaching task cannot distinguish information related to the visual target versus information related to movement planning, as there is a one-to-one correspondence between the instructed target and the upcoming movement direction. To disambiguate the nature of the information revealed in the LFP, we trained two monkeys to perform a 'choice task' consisting of two visual targets (in opposite directions) selected from the original eight on each trial. On each trial, the monkey was presented with two targets simultaneously and was required to make a choice to move to one of them. For all pairs of oppositely positioned targets presented simultaneously (**Fig. 8a**), we computed the mutual information between the phase (latency) of the LFP and the chosen movement direction (averaged over all pairs of simultaneously presented targets) across time during the instruction epoch in MI (**Fig. 8b**) and PMd (**Fig. 8c**). No evidence of transient information was found during the evoked wave, suggesting that the information in the LFP reflected the visual target and not the planned movement direction. As a control, information was computed between the phase of the LFP and movement direction for different pairs of targets presented on separate trials (**Fig. 8d**). We observed significant modulation in information 50–200 ms after the onset of the instruction signal for both MI (**Fig. 8e**) and PMd (**Fig. 8f**), as expected given the difference in visual stimuli.

DISCUSSION

Wave-like spatiotemporal activity is observed in the oscillatory behavior of the nervous system and is thought to be pivotal in computation and communication between subsystems of the brain[12]. Wave-like behavior occurs in various intact and semi-intact preparations, including the olfactory system of invertebrates[13] and vertebrates[14,15] and the turtle visual cortex[16–21]. Slice work has yielded insight into the potential of tissue to spontaneously generate propagating activity and sustain propagation evoked by stimulation, as observed in the guinea pig somatosensory cortex and rat barrel cortex[22,23]. The cortices of both the rat and cat are sensitive to $GABA_A$ antagonists, such as bicuculline, and

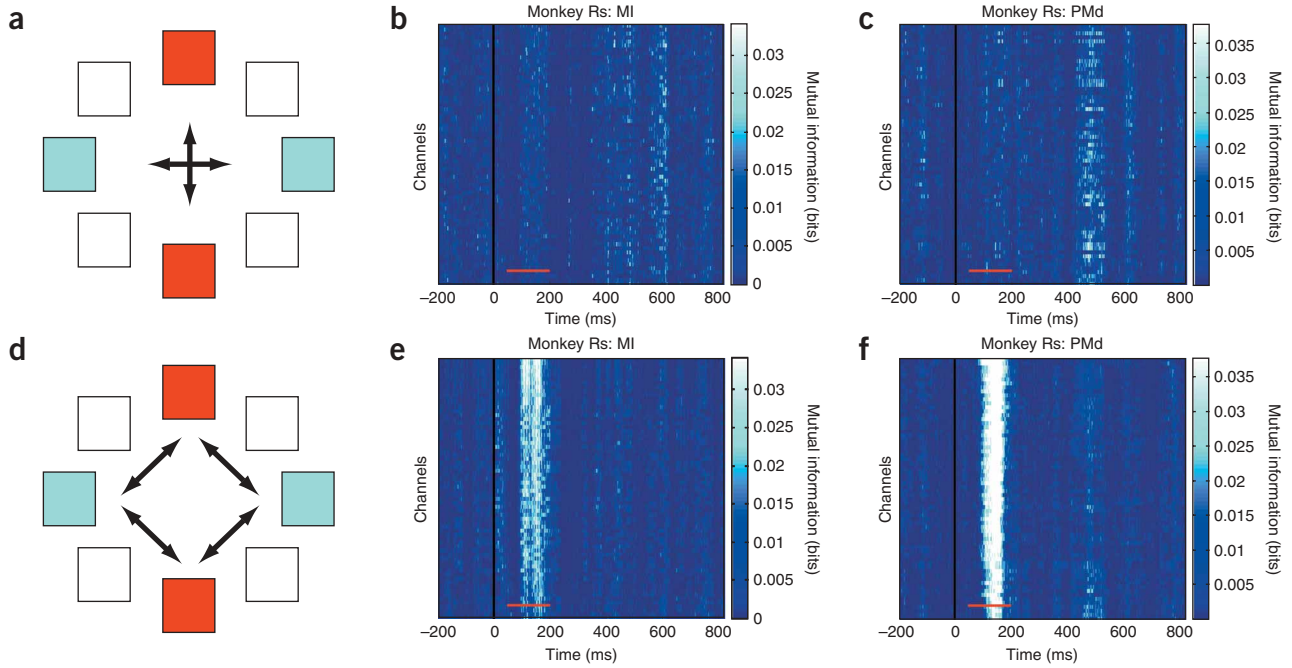

Figure 8 Target versus movement direction information. The data are computed from the choice task (Methods). (**a**) A schematic of two of the four pairs of targets presented in the task and the information calculation presented in **b**,**c**. On any given trial of the choice task, two targets appeared 180° apart (for example, the red or blue targets), and the monkey chose to reach for one of them. Information was computed between the wave phase of the LFP and the chosen movement direction (for example, left versus right movements or up versus down movements; arrows). (**b**,**c**) Mutual information between wave phase and the chosen movement direction in the choice task. Information values were computed across all trials corresponding to a single pair of simultaneously presented targets and then averaged over all pairs of targets. Time with respect to the instruction is presented on the horizontal axis, channels on the vertical axis. Wave-phase information is presented in blue-white false color in bits. The horizontal red dash marks the 50–200 ms containing the evoked potentials. The center value of the color axis was set to be the computed significant information threshold ($P = 0.01$). Data are from monkey Rs, MI (**b**) and monkey Rs, PMd (**c**). (**d**–**f**) Same as in **a**–**c**, with information computed between wave phase and chosen movement direction across different trial types (for example, left versus up movements; arrows) and then averaged.

removal of only 10–20 % of the inhibition induces 6–9 cm s^{-1} stimulus-triggered propagatory behavior in cortical slices[24,25]. Patches of these cortical slices have preferred propagation directions that are mediated by excitatory horizontal connections in the cortex.

We observed similar phenomena in the beta oscillations of awake, behaving monkeys. Beta activity propagated continually as waves across the cortex, traveling at a range of speeds with a mean of ~16 cm s^{-1} and a mode closer to 12 cm s^{-1} across monkeys. This propagation of the beta oscillations was a robust phenomenon that was observed in all four monkeys in both MI and PMd. Different cortical areas showed different preferences for propagation directions, and these dominant propagation directions were consistent across time and monkey in both MI and PMd. In light of other work, these waves may be controlled by local or thalamic interactions that modulate local $GABA_A$ inhibition in the cortex and may be a characteristic of cortical tissue in general.

The exact function of the beta oscillations in the sensorimotor cortex has been the subject of intense debate but remains largely unknown. There are several well documented properties of beta oscillations, including an increase in power during times of motor planning, motor imagery and maintained postural configurations, and a tendency to attenuate during periods of active, planned movement in both human and non-human primates[1,4–7]. Transient beta bursts are observed during tasks when primates actively search for their reward, which argues for the idea that beta oscillations are indicative of a heightened state of attention or global arousal[8–10].

On the other hand, EMG activity observed during the maintenance of a posture such as a precision grip task is phase-locked to cortical beta oscillations in the macaque motor cortex, and increased beta activity is correlated with slower movements[2,3]. These results suggest that beta oscillations may be more integrally related to muscle behavior, such as co-contraction during postural maintenance, and not indicative of the cognitive state of the animal at all.

We propose an account in which beta oscillations mediate intra- and inter-cortical communication. Within a cortical area, we observed evoked propagating waves whose latencies and amplitudes provided task-related information that traveled along the dominant propagation axis of the ongoing LFP waves. We speculate that the different dominant propagation axes of beta oscillations in MI and PMd are a consequence of the intrinsic interconnectivity within two functional networks: 1) an anterior-posterior network, consistent with the horizontal connectivity between MI and premotor cortex anteriorly and between MI and somatosensory cortex posteriorly[26–29], and 2) a medial-lateral network within area Brodmann area 6, consistent with the anatomical connectivity between PMd and supplementary motor cortex medially and between PMd and caudal portions of ventral premotor cortex laterally[30–32]. Although suggestive, our data leave unresolved whether the propagating waves mediate information transfer across cytoarchitecturally defined cortical areas.

Attenuated beta waves continued to propagate during movement execution, although they did not contain any information that was time locked to either the go cue or the start of movement. Given the lack of phase-locking with respect to movement onset (data not shown), it would not be possible to reliably measure information (if it even exists) because our methods depend on the existence of phase-locking over

multiple trials with respect to a behavioral event. This leaves open the possibility that movement-related information is present in the beta activity if movement-related features in the beta activity vary in time from trial to trial. If the appropriate temporal alignment could be found, this information could be measured.

If our hypothesis that beta wave propagation subserves intra- and inter-cortical information transfer is correct, we speculate that a signature of this transfer will be evident on the single-unit level. This view of transcortical cortical communication in the beta range may serve as a model for local field potential activity in general and suggests the possibility that higher aspects of cortical communication and information transfer may best be understood with respect to the spatiotemporal characteristics of oscillatory activity.

METHODS

Animals and behavioral tasks. Four macaque monkeys (*Macaca mulatta*) were operantly trained to perform an instructed-delay, center-out reaching task. The task was performed via a two-link exoskeletal robotic arm on which the monkey's arm was attached[33]. The position of the monkey's hand controlled the location of a cursor projected onto a horizontal screen above the monkey's arm. The animals were head-fixed to prevent movement artifacts. These experiments included four animals, termed monkeys B, R, Rs and Rx.

The instructed-delay center-out task consisted of three periods, referred to as the hold, instruction and movement periods. During the hold period, the monkey was trained to hold the cursor on a center target and wait 500 ms for the instruction cue. During the instruction period, the monkey was presented with one of eight evenly spaced peripheral targets and continued to hold at the center for an additional 1,000–1,500 ms. At that time, the go cue was presented, signaling the monkey to begin movement to the peripheral target. The monkey completed the trial successfully upon reaching the target and was given a juice or water reward.

Two of the animals were also trained to perform a second task, referred to as the 'choice task', designed to disassociate neural activity related to target versus movement direction. The task introduced a forced choice by instructing two targets instead of one. These targets were 180° apart and were selected from the original eight. The monkey could choose which target to move to and was rewarded for either, though the reward was higher for the target less frequented. Unequal rewards were instituted to prevent perseveration.

Electrophysiology. Each monkey was implanted with a multi-electrode array in either the arm area of the dorsal premotor cortex (PMd), the arm area of the primary motor cortex (MI) or both. The array was composed of 100 electrodes arranged in a 10 × 10 matrix with an inter-electrode distance of 400 microns (Cyberkinetics Neurotechnology Systems). All local field potentials (LFPs) were amplified with a gain of 5000, recorded digitally with a sampling rate of 1 kHz per channel, and digitally band-pass filtered from 0.30–250 Hz or 0.30–500 Hz using a Cerebus acquisition system (Cyberkinetics Neurotechnology Systems).

LFP data were post-processed by removing all unsuccessful trials and all channels with obviously errant means or standard deviations. These channels might not be functional due to broken electrodes, head-stage amplifiers or other sources of extreme noise. Each dataset used for analysis represented a set of simultaneously recorded LFPs from an array on one recording session and contained between 300 and 700 trials. A total of 23 datasets were analyzed (12 from PMd and 11 from MI) over four monkeys. In monkey Rs, three of the datasets from MI were recorded simultaneously with three datasets from PMd. All of the surgical and behavioral procedures were approved by the University of Chicago Institutional Animal Care and Use Committee and conform to the principles outlined in the Guide for the Care and Use of Laboratory Animals (NIH publication no. 86-23, revised 1985).

Analysis. All algorithms were implemented in Matlab®. Unless otherwise indicated, the instruction epoch refers to the 800 ms interval following the onset of the instruction cue.

The power spectrum for each channel was computed separately for the instruction epoch of each trial using a fast Fourier transform (FFT). The spectra were then averaged to produce the power spectrum of the instruction period. Time-frequency spectrograms were computed using the continuous wavelet transform with complex Morlet wavelet family scales[34] corresponding to wavelet center frequencies [1..100]. In contrast to standard FFT spectrograms using fixed time windows, the wavelet spectrogram uses longer time windows (larger scale) for lower frequencies than for higher ones. All temporal filtering was done by applying an 8th order 10 to 45 Hz Butterworth filter forward and backward in time to prevent phase distortion.

We applied the Hilbert transform to extract instantaneous phase and amplitude attributes[35]. The Hilbert transform (*Hb*) of a real signal can be computed by convolving the signal with $1/\pi$ in the time domain or by performing the equivalent operations in the frequency domain. $s(t) + iHb[s(t)] = a(t)e^{i\varphi(t)}$ is called the analytic signal of a real signal *s*. The instantaneous phase of $s(t)$ is $\varphi(t)$, the instantaneous amplitude is $a(t)$, and the instantaneous frequency is $d\varphi/dt$.

For each trial, we band-pass filtered each channel of the local field potential in a 1 s portion from 200 ms before the instruction cue to 800 ms following the instruction cue to obtain $V(x,y,t)$, the local beta field potential at point (x, y) on the array at time *t*. We applied the Hilbert transform *Hb* to the signal on each (x, y) channel to obtain the instantaneous amplitude $a(x,y,t)$ and the instantaneous phase, $\varphi(x,y,t)$:

$$V(x,y,t) + iHb[V(x,y,t)]) = a(x,y,t)e^{i\varphi(x,y,t)} \quad (1)$$

To unwrap the phase for display purposes, we assumed that the phases across the array at a single time step were within 2π of each other. Let φ be $\varphi - \bar{\varphi}$ wrapped into $[-\pi,\pi]$ using the tangent function. $\bar{\varphi}$ is the spatial average of the wrapped phase at a fixed time. The unwrapped phase is computed as $\varphi_{new} = \phi + \bar{\varphi}$. This unwrapped phase was also used for the phase gradient computation. Average phase maps were computed by spatially unwrapping the phase at each time point as just described and then subtracting the phase value of a reference electrode at that time before averaging. Note that phase need only be unwrapped in one dimension at a time to compute the derivatives for phase gradient calculations.

We defined the velocity of coherent activity to be the velocity of the contours of constant phase[36]. Let $\varphi(x,y,t)$ be the phase of beta activity at time *t* and coordinates *x* and *y* of the multi-electrode array. The velocity, $\mathbf{v} = (dx/dt, dy/dt)$ was computed by taking the total derivative of $\varphi(x,y,t) = c$ with respect to time:

$$d\varphi/dt = \nabla\varphi \cdot \mathbf{v} + \partial\varphi/\partial t = 0 \quad (2)$$

The velocity direction, which is perpendicular to the phase contours, is $-\nabla\varphi$. The velocity magnitude or speed is $\frac{\partial\varphi}{\partial t} \Big/ \|\nabla\varphi\|$.

Velocity is only well defined when the phase gradient is not zero and when the signal exhibits a 'coherent' propagation direction. We define the phase gradient directionality, $PGD(t)$, to measure how well phase gradients align across the array as a function of time:

$$PGD(t) = \left\|\overline{\nabla\varphi}\right\| \Big/ \overline{\|\nabla\varphi\|} \quad (3)$$

The bar denotes the spatial average at a fixed time. If the phase gradients at all spatial points on the array align at time *t*, $PGD(t)$ will be 1. On the other hand, if the phase gradients are randomly distributed, *PGD* will be close to 0. Estimates of wave direction and speed were based on times for which $PGD(t) > 0.5$. When the phase gradients are well-aligned across the array, the direction of the velocity is well estimated by $-\overline{\nabla\varphi}$ and the speed by

$$speed(t) = \left|\overline{(\partial\varphi/\partial t)}\right| \Big/ \overline{\|\nabla\varphi\|} \quad (4)$$

The PGD criterion eliminated the need to impose a threshold on the phase gradient magnitude when computing the velocity. PGD cannot detect the presence of radial waves propagating away from or toward an epicenter, but visual inspection suggests that this is not a relevant feature in our data. To verify that wave-like activity was most prevalent in the beta frequency range, we computed the average *PGD* (averaged over all trials and times) on LFP data band-pass filtered in 10 Hz bands from 0 to 100 Hz and determined that the average *PGD* peaked within 10 and 45 Hz (**Fig. 3b**).

The spatial coherence, which is based on space-frequency analysis[17], is an alternative measure of how wave-like a signal is. Let $V_{x,t}$ be the measured LFP

on channel x at time t. The LFP in the frequency band $[f - W, f + W]$ and the time interval [1 … T] was isolated using the following projection:

$$\tilde{V}_{x,k}(f) = \sum_{t=1}^{T} V_{x,t} e^{i2\pi ft} w_{t,k}(W) \quad (5)$$

Multiplication by $e^{i2\pi ft}$ shifts frequencies by $-f$. $w_{t,k}(W)$ is the k^{th} Slepian function[37] at time t and bandwidth W. The Slepians are orthogonal time basis functions that capture contributions in different parts of the time window in the frequency band [–W,W]. Frequencies are scaled by the sampling frequency and lie in [0, 0.5]. There are $K = floor\ (2WT)$ Slepians available at resolution bandwidth $2W$. The $\tilde{V}_{x,k}(f)$ are the elements of the M' K matrix $\tilde{\mathbf{V}}(f)$, where M is the number of channels in the multi-electrode array.

A necessary (but not sufficient) condition for wave-like activity in time interval [1 … T] and frequency band $[f - W, f + W]$ is that the Slepian projections (equation (5) are highly correlated[17], a condition that can be tested using the singular value decomposition:

$$\tilde{\mathbf{V}}(f) = \mathbf{F}(f)\Lambda(f)\mathbf{G}'(f)$$

The matrices $\mathbf{F}(f)$, $\Lambda(f)$ and $\mathbf{G}(f)$ are M' M, M' K and K' K matrices, respectively. The singular values, $\lambda_i(f)$, lie on the diagonal of $\Lambda(f)$. Typically $M > K$, and K determines the number of nonzero singular values. The coherence is defined by

$$C(f) = \lambda_1(f)^2 \Big/ \sum_{k=1}^{K} \lambda_k(f)^2 \quad (6)$$

$C(f)$ is one for a completely coherent response. Spatial coherence effectively measures how spatially stereotyped the signal is over a time window of length T in the frequency band $[f - W, f + W]$. We calculated the coherence as a function of frequency with a bandwidth W of ± 0.005 (± 5 Hz unscaled) for 300 ms windows chosen at random from the instruction periods of the trials. $K = 3$. The coherence was averaged across time windows and used to select a frequency band that included the spatially coherent activity of interest across all monkeys. We found this window to be from 10 to 45 Hz in the beta frequency range.

Previous researchers[17] estimated the phase from $\mathbf{F}_1$ (the first column of $\mathbf{F}$ in the space-frequency SVD) remapped as a complex image to physical coordinates of the array. Because of the short duration of the beta waves, we used the instantaneous phase computed from the Hilbert transform for the velocity calculations (**Supplementary Fig. 2**).

To quantify the locking of the signal to a behavior cue, we define the percent phase locking[35] at position (x, y) on the array at time t as

$$PPL(x, y, t) = 100[1 - H(\varphi(x, y, t))/H_{\max}] \quad (7)$$

$\varphi(x,y,t)$ is defined in equation (1). H is the Shannon entropy:

$$H(x, y, t) = -\sum_{k=1}^{N} p_k \log_2(p_k) \quad (8)$$

where N is the number of trials and p_k is the fraction of values of $\varphi(x,y,t)$ at fixed x, y, and t that lie within the kth bin. $H_{max} = \log_2(N)$. We used 5 bins for the calculation. $PPL(x,y,t)$ conveys the degree of certainty in the phase angles at a single location in space and time. PPL is zero if the LFP phase angles are randomly distributed at a given location in space and time and 100 if they are identical. PPL can therefore be used across space as a measure indicating the presence of an evoked potential at each time in the task. If the phase image of this evoked potential at a given time has wave characteristics and therefore a meaningful velocity, then the evoked signal is necessarily wave-like in nature.

We evaluated the information content of the waves using the mutual information between the behavioral cue (target direction) and a characteristic of the wave (propagation direction, propagation speed, amplitude, or phase at a particular channel and time). Mutual information is defined as[38]

$$I(X, Y) = H(X) - H(X|Y) \quad (9)$$

for random variables X and Y. $H(X)$ is the Shannon entropy as defined in equation (8) and $H(X|Y)$ is defined by

$$H(X|Y) = \sum_{y} p(y) \left[\sum_{x} p(x|y) \log_2 p(x|y) \right] \quad (10)$$

$p(x|y)$ is the conditional probability of X taking on the value x given that Y has the value y. $I(X,Y)$ is always non-negative and equals zero only if the uncertainty of X is not reduced by knowledge of Y. For this paper, Y represents the target directions. Y takes on one of eight possible values for the instructed-delay, center-out task.

X is a random variable representing an attribute of the signal such as the phase. Information conveyed by phase was computed using the distribution of $\varphi(x,y,t)$ at fixed x, y, and t over all trials. To compute the information conveyed by amplitude, we estimated the amplitude at fixed j and t over all trials. Using equation (1), we binned the amplitudes $a(x,y,t)$ in the 40 ms time window centered at t into 10 bins based on their phase value. $\varphi(x,y,t)$ was adjusted modulo 2π before determining the bin.

We also estimated information in wave speed and wave direction as a function of time using speed given by equation (4) and direction given by $-\overline{\nabla\varphi}$ for those times at which $PGD(t) > 0.5$. Because speed and direction did not contain significant information, these results were not displayed in the paper. To account for biases in estimating information from limited data, the target direction labels were randomly shuffled across all trials so that a trial originally associated with target direction i could be assigned one of the eight target directions by randomly interchanging the target direction labels. Mutual information was then computed between target direction and a feature of the LFP wave at each time point. The mean information from twenty shuffles was subtracted from the estimated information values that are presented in **Figures 7** and **8**.

The random shuffling procedure described above was also used to assess statistically significant information. The mean and standard deviation of the twenty shuffled estimates of information were first computed. By assuming a normal distribution of information values among the shuffles, an information value associated with $P < 0.01$ was found. For example, when X represented the phase, $\varphi(x,y,t)$, this computation produced a significant information threshold for each x, y and t. However, to scale the color map in **Figures 7** and **8** with a single significance threshold, we applied a second method for assessing statistically significant information. We computed the distribution of information, I, over all x, y and t during a 200 ms time interval before the onset of the instruction cue. Again, by assuming a normal distribution of information values before the instruction cue onset, the mean and standard deviation of the information values generated a single significant information threshold. The significance values computed by the first method were nearly identical to the single threshold determined by the second method.

Note: Supplementary information is available on the Nature Neuroscience website.

ACKNOWLEDGMENTS

We thank Z. Haga, D. Paulsen and J. Reimer for help with surgical implantation of the arrays, training of monkeys and data collection. We also thank M. Fellows, E. Gunderson and R. Penn for help with surgical procedures. This work was supported by a grant from the Whitehall foundation and a grant R01 NS45853-01 from the US National Institute of Neurological Disease and Stroke, both awarded to N.G.H. K.A.R. received support from a Research Centers in Minority Institutions grant 2G12RR1364-06A1 from the National Center for Research Resources at the US National Institutes of Health.

COMPETING INTERESTS STATEMENT

The authors declare that they have competing financial interests (see the *Nature Neuroscience* website for details).

Published online at http://www.nature.com/natureneuroscience
Reprints and permissions information is available online at http://npg.nature.com/reprintsandpermissions/

1. Sanes, J.N. & Donoghue, J.P. Oscillations in local field potentials of the primate motor cortex during voluntary movement. *Proc. Natl. Acad. Sci. USA* **90**, 4470–4474 (1993).
2. Baker, S.N., Kilner, J.M., Pinches, E.M. & Lemon, R.N. The role of synchrony and oscillations in the motor output. *Exp. Brain Res.* **128**, 109–117 (1999).
3. Gilbertson, T. *et al.* Existing motor state is favored at the expense of new movement during 13–35 Hz oscillatory synchrony in the human corticospinal system. *J. Neurosci.* **25**, 7771–7779 (2005).
4. Pfurtscheller, G., Graimann, B., Huggins, J.E., Levine, S.P. & Schuh, L.A. Spatio-temporal patterns of beta desynchronization and gamma synchronization in corticographic data during self-paced movement. *Clin. Neurophysiol.* **114**, 1226–1236 (2003).

5. Pfurtscheller, G., Krausz, G. & Neuper, C. Mechanical stimulation of the fingertip can induce bursts of beta oscillations in sensorimotor areas. *J. Clin. Neurophysiol.* **18**, 559–564 (2001).
6. Pfurtscheller, G., Neuper, C., Brunner, C. & da Silva, F.L. Beta rebound after different types of motor imagery in man. *Neurosci. Lett.* **378**, 156–159 (2005).
7. Donoghue, J.P., Sanes, J.N., Hatsopoulos, N.G. & Gaál, G. Neural discharge and local field potential oscillations in primate motor cortex during voluntary movements. *J. Neurophysiol.* **79**, 159–173 (1998).
8. Murthy, V.N. & Fetz, E.E. Coherent 25- to 35-Hz oscillations in the sensorimotor cortex of awake behaving monkeys. *Proc. Natl. Acad. Sci. USA* **89**, 5670–5674 (1992).
9. Murthy, V.N. & Fetz, E.E. Oscillatory activity in sensorimotor cortex of awake monkeys: synchronization of local field potentials and relation to behavior. *J. Neurophysiol.* **76**, 3949–3967 (1996).
10. Murthy, V.N. & Fetz, E.E. Synchronization of neurons during local field potential oscillations in sensorimotor cortex of awake monkeys. *J. Neurophysiol.* **76**, 3968–3982 (1996).
11. O'Leary, J.G. & Hatsopoulos, N.G. Early visuomotor representations revealed from evoked local field potentials in motor and premotor cortical areas. *J. Neurophysiol.* **96**, 1492–1506 (2006).
12. Ermentrout, G.B. & Kleinfeld, D. Traveling electrical waves in cortex: Insights from phase dynamics and speculation on a computational role. *Neuron* **29**, 33–44 (2001).
13. Delaney, K.R. *et al.* Waves and stimulus-modulated dynamics in an oscillating olfactory network. *Proc. Natl. Acad. Sci. USA* **91**, 669–673 (1994).
14. Lam, Y.-W.L., Cohen, L.B., Wachowiak, M. & Zochowski, M.R. Odors elicit three different oscillations in the turtle olfactory bulb. *J. Neurosci.* **20**, 749–762 (2000).
15. Friedrich, R.W., Habermann, C.J. & Laurent, G. Multiplexing using synchrony in the zebrafish olfactory bulb. *Nat. Neurosci.* **7**, 862–871 (2004).
16. Senseman, D.M. & Robbins, K.A. High-speed VSD imaging of visually evoked cortical waves: decomposition into intra- and intercortical wave motions. *J. Neurophysiol.* **87**, 1499–1514 (2002).
17. Prechtl, J.C., Cohen, L.B., Pesaran, B., Mitra, P.P. & Kleinfeld, D. Visual stimuli induce waves of electrical activity in turtle cortex. *Proc. Natl. Acad. Sci. USA* **94**, 7621–7626 (1997).
18. Robbins, K.A. & Senseman, D.M. Extracting wave structure from biological data with application to responses in turtle visual cortex. *J. Comput. Neurosci.* **16**, 267–298 (2004).
19. Senseman, D.M. & Robbins, K.A. Modal behavior of cortical neural networks during visual processing. *J. Neurosci.* **19**, RC3 (1999).
20. Wang, W., Campaigne, C., Ghosh, B.K. & Ulinski, P.S. Two cortical circuits control propagating waves in visual cortex. *J. Comput. Neurosci.* **19**, 263–289 (2005).
21. Du, X., Ghosh, B.K. & Ulinski, P. Encoding of motion targets by waves in turtle visual cortex. *IEEE Trans. Biomed. Eng.* **53**, 1688–1695 (2006).
22. Contreras, D. & Llinas, R. Voltage-sensitive dye imaging of neocortical spatiotemporal dynamics to afferent activation frequency. *J. Neurosci.* **21**, 9403–9413 (2001).
23. Wu, J.Y., Guan, L. & Tsau, Y. Propagating activation during oscillations and evoked responses in neocortical slices. *J. Neurosci.* **19**, 5005–5015 (1999).
24. Chervin, R.D., Pierce, P.A. & Conners, B.W. Periodicity and directionality in the propagation of epileptiform discharges across neocortex. *J. Neurophysiol.* **60**, 1695–1713 (1988).
25. Chagnac-Amitai, Y. & Conners, B.W. Horizontal spread of synchronized activity in neocortex and its control by GABA-mediated inhibition. *J. Neurophysiol.* **61**, 747–758 (1989).
26. Muakkassa, K.F. & Strick, P.L. Frontal lobe inputs to primate motor cortex: evidence for four somatotopically organized 'premotor' areas. *Brain Res.* **177**, 176–182 (1979).
27. Kurata, K. Corticicortical inputs to the dorsal and ventral aspects of the premotor cortex of macaque monkeys. *Neurosci. Res.* **12**, 263–280 (1991).
28. Cauller, L.J., Clancy, B. & Connors, B.W. Backward cortical projections to primary somatosensory cortex in rats extend long horizontal axons in layer I. *J. Comp. Neurol.* **390**, 297–310 (1998).
29. Luppino, G. & Rizzolatti, G. The organization of the frontal motor cortex. *News Physiol. Sci.* **15**, 219–224 (2000).
30. Luppino, G., Matelli, M., Camarda, R.M. & Rizzolatti, G. Corticocortical connections of area F3 (SMA-proper) and area F6 (pre-SMA) in the macaque monkey. *J. Comp. Neurol.* **338**, 114–140 (1993).
31. Ghosh, S. & Gattera, R. A comparison of the ipsilateral cortical projections to the dorsal and ventral subdivisions of the macaque premotor cortex. *Somatosens. Mot. Res.* **12**, 359–378 (1995).
32. Dum, R.P. & Strick, P.L. Frontal lobe inputs to the digit representations of the motor areas on the lateral surface of the hemisphere. *J. Neurosci.* **25**, 1375–1386 (2005).
33. Scott, S.H. Apparatus for measuring and perturbing shoulder and elbow joint positions and torques during reaching. *J. Neurosci. Methods* **89**, 119–127 (1999).
34. Muthukumaraswamy, S.D. & Johnson, B.W. Primary motor cortex activation during action observation revealed by wavelet analysis of the EEG. *Clin. Neurophysiol.* **115**, 1760–1766 (2004).
35. Quyen, M.L. *et al.* Comparison of the Hilbert transform and wavelet methods for the analysis of neuronal synchrony. *J. Neurosci. Methods* **111**, 83–98 (2001).
36. Fleet, D.J. & Jepson, A.D. Computation of component image velocity from local phase information. *Int. J. Comput. Vis.* **5**, 77–104 (1990).
37. Percival, D.B. & Walden, A.T. *Spectral Analysis for Physical Applications: Multitaper and Conventional Univariate Techniques* (Cambridge University Press, Cambridge, UK, 1993).
38. Cover, T. *Elements of Information Theory* (John Wiley & Sons, New York, 1991).